Eletrônica de Potência
Open Journal of Power Electronics

Received May 01, 2024; accepted July 09, 2024; Date of publication July 31, 2024.
The review of this paper was arranged by Associate Editor Allan F. Cupertino and Editor-in-Chief Heverton A. Pereira.

Digital Object Identifier http://doi.org/10.18618/REP.2005.2.037044

Hydro-PV Dispatchable Microgeneration: Proposal, Simulation and Modeling

Valdecir Junior De Paris[1], Fernanda de Morais Carnielutti[2], Denizar Cruz Martins[1]

[1]Federal University of Santa Catarina — UFSC, Department of Electrical Engineering, Florianópolis, SC, Brazil
[2]Federal University of Santa Maria — UFSM, Department of Eletrical Energy Conversion, Santa Maria, RS, Brazil

e-mail: deparis.vj@gmail.com, fernanda.carnielutti@gmail.com, denizar.martins@gmail.com

ABSTRACT The increasing global demand for energy has popularized wind and solar photovoltaics, yet their reliance on climate conditions necessitates energy storage solutions like batteries or hydroelectric reservoirs. While large hydro projects face high costs and stringent regulations, hydro microgeneration systems offer a cost-effective alternative with reduced environmental impact. This paper introduces a microgrid design incorporating three converters combining solar PV and hydro sources, meeting grid standards. It presents the system's design, control methods, and validation through hardware-in-the-loop testing. The proposed Hydro-PV microgeneration system outperforms standard systems, especially during rainy periods, by ensuring off-grid operation without the need for additional batteries due to its dispatchable characteristics. This innovative approach enhances sustainability, efficiency, and grid compatibility while optimally utilizing both hydro and photovoltaic resources. Furthermore, the average model developed in the paper can be used to compare this method's benefits regarding battery storage in different regions.

KEYWORDS Hybrid-generation, real-time-simulation, reservoir-control, storage-system, sustainability.

I. INTRODUCTION

Recent energy reports emphasize a significant increase in renewable energy investments, reaching approximately 85% of total electricity generation investments globally [1]. However, the integration of intermittent renewable sources, like wind and solar, poses challenges due to fluctuating energy output. Then, despite this surge, many countries still heavily rely on fossil fuels for power generation. To address this, additional Energy Storage Systems (ESS) such as batteries, hydrogen tech, or hydro reservoirs are crucial [2], [3].

Hybrid systems merging hydro and photovoltaic sources have been proposed, utilizing their complementary nature to ensure stable annual energy generation [4]. Furthermore, advancements in floating PV systems near water bodies have shown improved efficiency [5]. Moreover, optimizing control strategies for reservoir levels in large Hydro-PV systems enhances generation efficiency by storing excess energy for subsequent use [6]. These integrated systems hold significant potential for rural electrification initiatives, offering a spectrum of control strategies and configurations to ensure both technical robustness and economic viability [7]–[13].

In hydro-microgeneration systems, converters are often used instead of governor turbines for regulating voltage and frequency, particularly in areas with limited stream-flow and low power. This approach proves advantageous in areas where the expense of distribution lines outweighs that of operating a microgeneration system closes to consumption centers [14]–[17].

In this context, distributed generation (DG) systems are more efficient compared to centralized systems, which have high transmission losses and environmental concerns associated with the implementation of large power plants, among other issues. Adding renewable energy sources near consumer units, integrating loads into a common dc bus, and employing robust and stable controls are all related to the concept of dc microgrids. These integrate with the existing power grid as a single point, or they can operate autonomously, disconnected from the grid [18].

This paper introduces a hybrid microgeneration system that operates as a dc microgrid, integrating small stream-flow hydroelectric generation with PV and energy storage for continuous energy availability, achieved through the proposed reservoir control. The paper focuses on modeling the primary sources (hydro and PV), designing converter elements and controls, presenting simulation results, and conducting real-time hardware-in-the-loop testing. The aim is to provide a comprehensive understanding of the system's functionality and performance, establishing a baseline average model to guide future applications.

The paper is organized as follows: Section II presents the proposed system, including the modeling of primary sources and the design of the Hydro-PV system and reservoir. Section III details the design of the converter elements and control strategies. Section IV showcases real-time hardware-in-the-loop simulation results to verify the system's performance, along with an average model block diagram to facilitate reproducibility of the analysis.

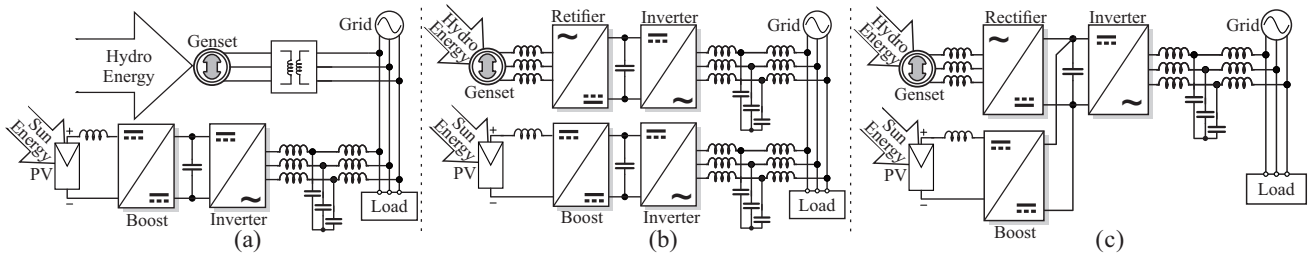

FIGURE 1. Power system circuits: (a) standard hybrid; (b) standard hybrid microgeneration; (c) proposed hybrid microgeneration.

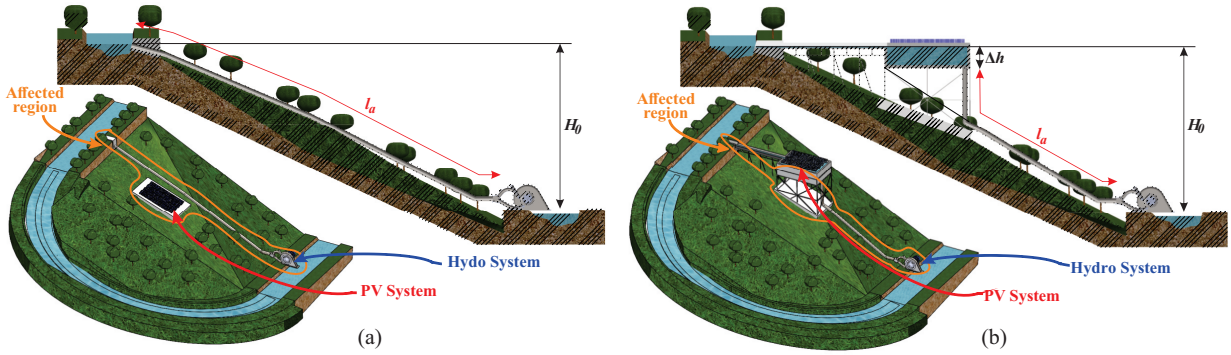

FIGURE 2. Illustration of the hybrid micropower system: (a) standard; (b) proposed.

II. PROPOSED SYSTEM

Power systems traditionally connect energy sources directly to the electrical grid based on weather or hydro conditions, as shown in Fig. 1 (a). In cases with limited or fluctuating hydropower (microgeneration), converters are necessary for improved efficiency due to hydro system speed/flow variations, that is depicted at Fig. 1 (b).

The topology shown in Fig. 1 (c) was applied in the proposed system, in which integrates both sources onto the same dc bus, well-known as dc microgrid [18], allowing the Hydro-PV system's higher generation levels in variable climatic conditions. This system uses a single inverter for both, the PV system and hydropower, maintaining consistent power output near the PV rated power system. It means that the inverter is the same used just in PV generation, avoiding additional inverters costs. Additionally, it takes advantage of the reservoir area for PV modules placement.

Fig. 2 shows that the proposed system's affected area is similar to that of the standard system, thus mitigating the usual environmental impact of hydropower reservoirs. However, a major drawback is the reservoir cost, which varies with geographic region characteristics and is difficult to evaluate. This cost should be weighed against the cost and sustainability of a battery energy storage system (BESS). Therefore, the geographic region characteristics could define, which one would be better.

For designing and simulating converters in the proposed system, understanding and modeling primary sources is essential. Parameters like water fall (H_0), stream flow (Q_r), irradiance (I_0), and ambient temperature (T_0) are key input data, to be converted to electrical data for simulation.

A. Hydro-system

For hydropower, the maximum power generated is defined by

$$P_{hy} = \rho \cdot g \cdot H_0 \cdot Q_r \cdot \eta, \tag{1}$$

where ρ is the water density and g the gravity constant, η represents the efficiency of the system. In hydro microgeneration, the losses in the pipeline (h_l) reduce the potential energy and consequently the water potential is defined by the effective height (H_e) presented by

$$H_e = H_0 - h_l. \tag{2}$$

The parameter h_l is influenced by pipeline characteristics like length (l_a), diameter (d_a), and friction factor (f_a). The hydro characteristics are crucial for selecting an ideal hydro turbine. As Pelton turbines are more efficient with higher head due to stored potential energy in a small area, it was defined to be used. The power generated by this turbine (P_{turb}) is defined as

$$P_{turb} = \rho \cdot Q_e \cdot c_1^2/2 = \omega_{turb} \cdot T_{mec}, \tag{3}$$

that is related to the speed of the water jet (c_1) at the injection nozzle, that depends on its loss coefficient K_n, and turbocharged flow (Q_e), presented as

$$c_1 = K_n \cdot \sqrt{2 \cdot g \cdot H_e}, \qquad Q_e = c_a \cdot \pi \cdot d_a^2/4. \tag{4}$$

The diameter of the injection nozzle d_n determines the power provided by the turbine P_{turb} and the flow Q_e demanded. Where it is possible to obtain the maximum power or operating point according to the variation of nozzle diameter, as shown in Fig. 3. By the definition of mass conservation, it is possible to relate the turbocharged flow

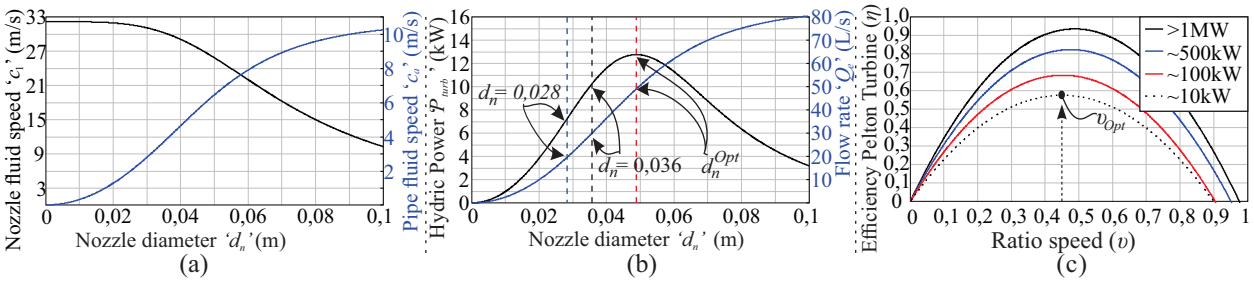

FIGURE 3. Waveforms of: (a) flow speed vs nozzle diameter; (b) flow rate and power vs nozzle diameter; (c) efficiency vs ratio speed.

to the nozzle and pipeline speeds (c_1, c_a), and diameters (d_n, d_a) by relation

$$c_a = c_1 \cdot (d_n/d_a)^2, \tag{5}$$

whose variation is shown in Fig. 3 (a). Frictional losses influence power variation with flow increase, reaching a maximum power point due to increased losses, reducing jet speed and power shown in Fig. 3 (b).

To define the genset to be used in hydro generation, it is necessary to obtain the electric relation with the speed (ω_{turb}) and torque (T_{mec}) available at the turbine shaft to feed the machine. Then, the generator current reference is obtained,

$$i_q^{ref} = \frac{2}{3} \cdot \frac{2}{N_{poles}} \cdot \frac{T_{mec}}{\psi_{pkm}}, \tag{6}$$

where the number of poles (N_{poles}) and concatenated magnetic flux (ψ_{pkm}) of a permanent magnet synchronous machine (PMSM) are necessary. The T_{mec} is obtained from the point of maximum efficiency as illustrated in Fig. 3 (c) which is related with (3) and the ratio speed υ, presented as

$$\upsilon = \frac{U}{c_1}, \tag{7}$$

in which U is the tangential speed of the turbine rotor, related with the generator speed. Thus, defining the maximum efficiency of the turbine and consequently the reference torque only with the jet speed and turbine data. Fig. 3 (c) also illustrates as example of the reduction in the efficiency of hydroelectric plants with the reduction of power [19].

B. PV-system

In photovoltaic solar energy, by knowing the latitude and climatic characteristics of the region, such as the luminosity (K_t) and diffuse (K_d) index, it is possible to estimate the annual photovoltaic power variation through the geometric relationships sun-earth-module [20].

The incident irradiance on the module ($I_{G\theta}$) is related to the place's direct (I_{DR}), diffuse (I_{DF}), and global (I_{GH}) irradiance by means of:

$$I_{G\theta} = I_{DR\theta} + I_{DF\theta}, \tag{8}$$

$$I_{DF\theta} = I_{DF}(Y_\theta \sin(\theta_\beta) + \cos(\theta_\beta)), \tag{9}$$

$$I_{DR\theta} = I_{DR}\cos(\theta_z), \tag{10}$$

$$I_{DR} = I_{GH} - I_{DF}, \quad I_{DF} = I_{GH}K_d, \quad I_{GH} = I_0 K_t. \tag{11}$$

In which the irradiances with the subscript θ are related to the module tilt angle (θ_β) and its azimuth (θ_w). The parameter (Y_θ) represents a diffuse condition related to the zenith angle (θ_z). The local rated irradiance (I_0) changes throughout the year as follows

$$I_0 = \frac{I_{sc}\,(1 + 0.33\cos(day/365))}{AM}, \tag{12}$$

where I_{sc} is the solar constant, and AM the air mass,

$$AM = \frac{1}{\sin(\theta_\alpha) + 0.50572(6.07995 + \theta_\alpha)^{-1.6364}}, \tag{13}$$

that is related to the solar incident angle (θ_α), which is defined by the place's latitude. The values of θ_α, as well as the irradiances, change throughout the hours and days.

Currently, meteorological laboratories' reports provide data of irradiances and ambient temperature (T_0). Thus, it is possible to estimate $I_{G\theta}$ using an analytical approach (8) or direct real data [21], and then determine the module's temperature T_{pv},

$$T_{pv} = T_0 + \frac{T^{ref} - 20}{800} \cdot I_{G\theta}. \tag{14}$$

Those are the data needed to obtain the value of available power at the output of the module (P_{pv}) defined by

$$P_{pv} = \frac{I_{G\theta}}{I_{G\theta}^{ref}} \cdot P_{max}^{ref}[1 + \alpha_{Pmax} \cdot (T_{pv} - T^{ref})], \tag{15}$$

that follow: module's maximum power temperature coefficient (α_{Pmax}); module's irradiance and temperature reference ($I_{G\theta}^{ref}$, T^{ref}); and maximum power PV system reference (P_{max}^{ref}).

The sizing of the photovoltaic system is based on the PV module's maximum power (P_{max}^{NOCT}), as well as voltage, and current at the maximum power point (v_{pmp}, i_{pmp}). The system's voltage and power reference (v_{pv}^{ref}, p_{pv}^{ref}) are project parameters. This criterion was used to obtain the number of modules in series (N_{spv}) and parallel (N_{ppv}) defined respectively by

$$N_{spv} = \left(\frac{v_{pv}^{ref}}{v_{pmp}}\right), \quad N_{ppv} = \left(\frac{p_{pv}^{ref}/v_{pv}^{ref}}{i_{pmp}}\right). \tag{16}$$

Subsequently, the reference maximum power of the system is obtained,

$$P_{max}^{ref} = P_{max}^{NOCT} \cdot N_{spv} \cdot N_{ppv}. \tag{17}$$

$$I_{G\theta}^{ref} = 800\text{W/m}^2; \quad T^{ref} = 47°\text{C}. \tag{18}$$

The $I_{G\theta}^{ref}$ and T^{ref} values (18) were defined under normal operating conditions, also known as normal operating cell temperature condition (NOCT). In which are manufacture's data parameters [20]. Fig. 4 represents the variation of the photovoltaic power generated according to the year in the west of Santa Catarina state (Brazil), defined by (15) in function of (14) and (8). These can also be validated according to meteorological laboratories, due to climatic variations and rain precipitation stochastic characteristics [21]–[23].

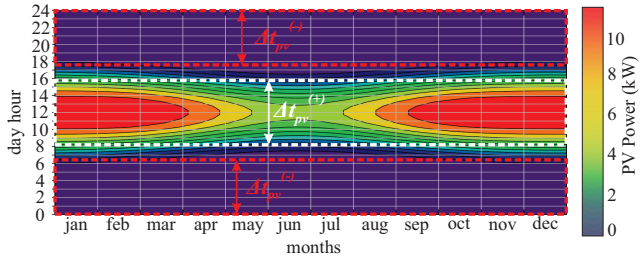

FIGURE 4. Power PV variation during the year (26º35'S 52º31'W).

C. Reservoir design methodology

The analytical result presented in Fig. 4 was used to sizing the area of the reservoir. Where $\Delta t_{pv}^{(+)}$ represent the average amount of time that the demand is supplied by photovoltaic energy. The night period, time during which the demand is met by hydropower, was presented as $\Delta t_{pv}^{(-)}$. These parameters were used to calculate the reservoir area (A_r) by defining an operation level (Δh) and with the stream flow (Q_r) to get the maximum limit to fill the reservoir during the day according to

$$A_r^{max} < \frac{Q_r}{\Delta h} \cdot \Delta t_{pv}^{(+)}, \tag{19}$$

and with turbocharged (Q_e) to get the minimum limit to meet the load at night according to

$$A_r^{min} > \frac{Q_e - Q_r}{\Delta h} \cdot \Delta t_{pv}^{(-)}. \tag{20}$$

The reservoir area was obtained through the average value from (19) and (20), and the same method was used for the dynamic model of the reservoir, which represents the variation of the reservoir level (Δh) during the operating time (Δt) by means of

$$\frac{\Delta h}{\Delta t} = \frac{Q_r - Q_e}{A_r}. \tag{21}$$

Fig. 5 shown a comparative between hydrological scenarios, altering area based on height and stream flow for the same power, to show that high height's affected area is similar to photovoltaic systems. Although low-head systems are unsuitable for Pelton turbines, the picture emphasizes that the proposed benefits are only achievable with high head conditions. Even with Francis or Kaplan turbines, the required area would be significantly larger compared to that of a PV system, compromising the intended sustainability due to the increased environmental affected area.

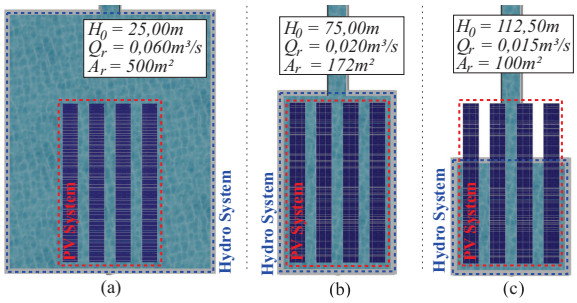

FIGURE 5. Comparison of affected area in PV and Hydro system with 10 kW power system: (a) low-height; (b) medium-height; (c) high-height.

III. CONVERTERS AND CONTROLS

The complete power circuit of the proposed system is presented in Fig. 6 and the data obtained in the design of the components and main parameters used in the system are presented in Table 1. The proposed system uses three converters, i.e, a boost converter, an active rectifier and an inverter. The design of its components followed well-known methodologies in the literature and industry [24], [25].

A. Converters parameters

The boost converter for photovoltaic solar generation is responsible for tracking maximum power and suitability with the bus voltage. Its main component, the inductor, is designed according to

$$L_{Boost} = \frac{V_{pv} \cdot D_{Boost}}{f_s \cdot \Delta i}. \tag{22}$$

The active rectifier is connected to the hydro generation to adapt the ac generator output voltage to the dc bus voltage level, whose inductor and bus capacitor follow

$$L_{Ret} = \frac{V_{hy} \cdot \sqrt{2}}{f_s \cdot \Delta i} \cdot \left(1 - \frac{3}{2} \cdot \frac{V_{hy} \cdot \sqrt{2}}{V_{dc}}\right), \tag{23}$$

$$C_{dc} = \frac{2 \cdot P_0 \cdot t_{hu}}{V_{dc}^2 - V_{min}^2}. \tag{24}$$

Finally, the inverter for grid connection was designed to respect the values of power factor (PF) and total harmonic distortion (THD) defined by grid codes and standards such as IEC 61000-3-12. Then, an LCL filter was used to reduce

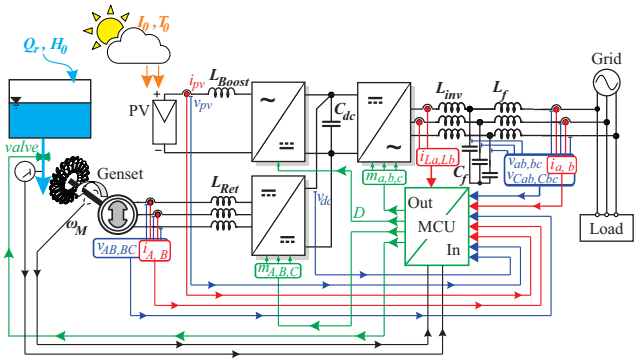

FIGURE 6. Proposed power and control circuit.

TABLE 1. Converter parameters [20]

Symbol	Description	Value
P_{pv}	*Boost* converter rated power	12 kW
P_{hy}	Genset rated power	11 kW
P_0	Inverter rated power	12 kW
f_{hy}	Genset rated frequency	90 Hz
V_{hy}	Genset (rms) rated line voltage	322 V
f_g	Grig rated frequency	60 Hz
V_{rms}	Grid (rms) rated line voltage	380 V
I_{rms}	Grid (rms) rated current	18.23 A
f_s	Switching frequency	10 kHz
V_{dc}	Bus voltage	600 V
V_{pv}	PV system output rated voltage	408 V
D_{Boost}	Boost rated duty cycle	0.324
Δi_{Boost}	Percent boost current ripple	10%
L_{Boost}	Boost inductor	4.49 mH
Δi_{Ret}	Percent rectifier current ripple	10%
L_{Ret}	Rectifier inductor	3.23 mH
V_{min}	Minimum bus voltage	570 V
t_{hu}	Hold-up-time	8.333 ms
C_{dc}	Bus capacitor	5.698 mF
ω_h	First angular harmonic frequency	62.2 krad/s
λ_{Vh}	Percent harmonic voltage magnitude	32.42%
Δi_{inv}	Percent inverter current ripple	20%
L_{inv}	Inverter side inductor	1.35 mH
λ_C	Percent reactive rate limit	5%
C_f	Filter capacitor	11.02 μF
λ_h	Percent of angular harmonic limit	0.2%
L_f	Filter inductor	0.78 mH

the high order current harmonic from the inverter, in which the inverter's side inductor of the filter was defined by

$$L_{inv} = \frac{V_{rms} \cdot \sqrt{2}}{f_s \cdot \Delta i} \cdot \left(1 - \frac{3}{2} \cdot \frac{V_{rms} \cdot \sqrt{2}}{V_{dc}}\right), \tag{25}$$

and the values of the filter capacitor and grid inductor are obtained through

$$C_f = \frac{\lambda_C \cdot P_0}{2\pi \cdot f_g \cdot V_{rms}^2}, \tag{26}$$

$$L_f = \frac{1}{L_{inv} \cdot C_f \cdot \omega_h^2 - 1} \cdot \left(L_{inv} + \frac{\lambda_{Vh} \cdot V_{dc}}{\omega_h \cdot \lambda_h \cdot I_{rms}^2}\right). \tag{27}$$

The current ripple values (Δi), reactive rate (λ_C) and harmonic limit (λ_h) followed common values used in the industry. As well as the definition of the bus voltage (V_{dc}) and switching frequency (f_s).

B. Controllers parameters

The entire control system is implemented using a single microcontroller (MCU), interfacing with the sensors as indicated by the arrows in Fig. 6. The control is detailed in Fig. 7 where each color represents a control strategy applied, presented in this section, whose results are in Table 2. The control system bases in established theories, wherein control strategies are drawing upon prior research [26]–[28].

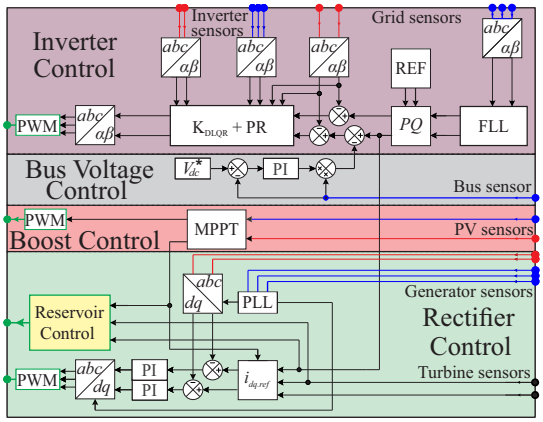

FIGURE 7. Proposed MCU's general control block diagram.

The inverter control, used to regulate the current injected into the grid, make use of a proportional resonant control (PR). The stationary transform $\alpha\beta$ was employed, allowing independent axis control, that helps the bus voltage control. Inverter synchronization is achieved through a frequency-locked loop (FLL) to dimension controllers and obtain current references in $\alpha\beta$ without requiring phase angle information.

Digital linear quadratic regulator (DLQR) methodology is employed to determine state feedback gains (K_{DLQR}) for the inverter controllers. This approach facilitates direct discrete-time control while accounting for digital delays in the system. It aids in controlling the rejection of low-order harmonics inherent in the electrical grid. Consequently, inverter modulating signals (m_{abc}) are computed based on grid voltage and current values (v_{abc}, i_{abc}), voltage and current in the inverter elements (v_{Cabc}, i_{Labc}, v_{dc}), and power references (P_{ref}, Q_{ref}). Fig. 8 zoomed the K_{DLQR}+PR block from Fig. 7, where the PR controllers follow the second order transfer function for each harmonic

$$G_h(z) = \frac{1 - \cos(\omega_r t) z^{-1}}{1 - 2e^{-\lambda_r T_a} \cos(\omega_r t) z^{-1} + e^{-2\lambda_r T_a} z^{-2}}, \tag{28}$$

in which T_a is the sample period, ω_r the resonance frequency and λ_r is related with the damping factor [20], [26]. The PR controller is derived from a cosine function, resulting in two states for each PR designed. The state feedback gain for each PR harmonic, delay, and converter parameters are highlighted in blue in the Fig. 8, whose values are in Table 2.

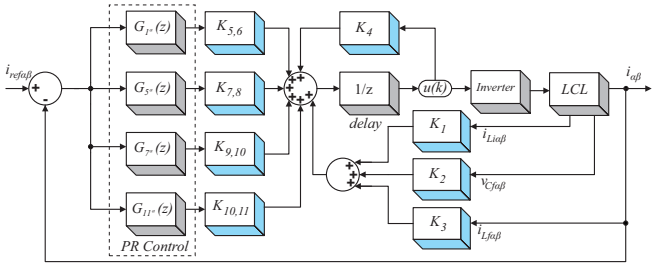

FIGURE 8. K_{DLQR}+PR block control details.

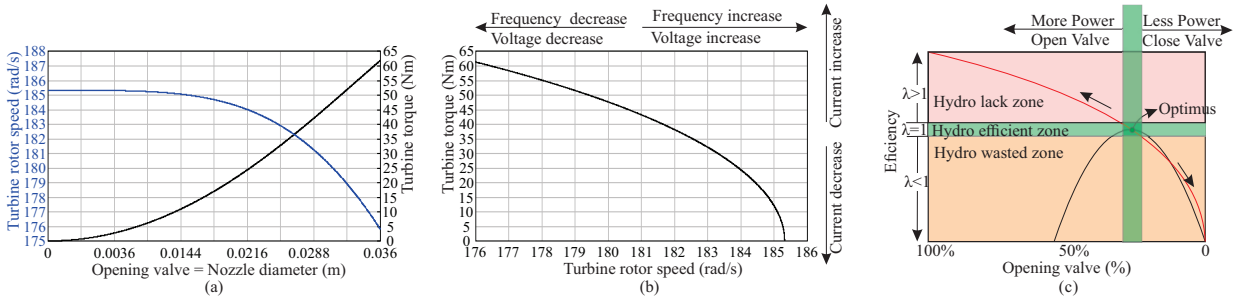

FIGURE 9. Waveforms of: (a) torque and speed vs diameter of nozzle; (b) torque vs speed; (c) illustration of valve control algorithm.

TABLE 2. Control parameters [20]

Symbol	Description	Value
K_1	Current i_{Li} gain	6.0625
K_2	Voltage v_{Cf} gain	-0.5684
K_3	Current i_{Lf} gain	-3.3695
K_4	Delay ϕ gain	0.2492
$K_{5,6}$	1^o, 2^o state PR fundamental gain	$0.0610, -0.0614$
$K_{7,8}$	1^o, 2^o state PR 5^a harmonic gain	$0.0035, -0.0029$
$K_{9,10}$	1^o, 2^o state PR 7^a harmonic gain	$0.0006, -0.0003$
$K_{11,12}$	1^o, 2^o state PR 11^a harmonic gain	$-0.0001, 0.0002$
f_{ci}/ $M_{\phi i}$	Rectifier cut-off frequency/phase margin	1 kHz/65^o
τ_{zi}/ K_{ci}	Rectifier PI time constant / gain	0.0005/0.0325
f_{cv}/ $M_{\phi v}$	Bus cut-off frequency/phase margin	10 Hz/65^o
τ_{zv}/K_{cv}	Bus PI time constant / gain	0.0618/0.5568

The Rectifier control is achieved through synchronous transformation (dq) which represents a three-phase system with two constant values. This approach was chosen due to the varying generator frequency during operation. The constant values from the dq transformation enable current and power control using a proportional integral controller (PI) under various operating conditions, in which their controllers are designed in the frequency domain, by definition of a cut-off frequency and a phase margin.

A phase-locked loop (PLL) is employed to incorporate frequency into the control system for obtaining the values of the dq axis. Modulating signals (m_{ABC}) are derived from the generator voltages and currents (v_{abc}, i_{abc}), considering the dc bus voltage (v_{dc}) and current references (i_{dref}, i_{qref}).

The bus Voltage Control is implemented in an external loop, integrated into the control loop (α), in conjunction with the inverter, using a PI controller. The PI parameters for bus voltage control are determined using the same methodology used in rectifier control.

The boost control entails maximizing the power output of PV modules through perturb and observe technique. This primary control method involves altering the duty cycle D and monitoring power using voltage and current (v_{pv}, i_{pv}). The technique induces oscillations to seek the maximum power, comparing the current point with the previous one.

The reservoir control is a central aspect of this section, revolves around optimizing water utilization to maintain the reservoir level effectively. This optimization condition is formulated as

$$\lambda = \frac{P_{ret}}{P_{turb}}, \qquad P_{ret} = P_{ref} - P_{pv}. \tag{29}$$

wherein P_{ret} denotes the energy required by the rectifier, while P_{turb} signifies the energy supplied by the turbine. The power generated by the turbine relies on engine speed and torque (3). The control over the nozzle diameter is achieved by regulating the opening of the nozzle/valve on the Pelton turbine, as illustrated in Fig. 9 (a). Expressing torque as a function of engine speed, relative to the variation in valve opening, as depicted in Fig. 9 (b), the reservoir control logic is defined. Due to relationship between torque and generator current with respect to head, as well as voltage and frequency concerning engine speed and turbocharged flow. Fig. 9 (c) provides a visual representation of the efficiency curve for a condition where approximately 30% of hydropower is required.

IV. REAL-TIME SIMULATION

Fig. 10 show the Typhoon HIL 402 device used for real-time simulation, that also support long-term simulations, aiming to compare the the proposed and standard system. Real-time simulations help in the representation of the physical characteristics of the models, being able to represent slow and fast dynamics, as shown in Fig. 11.

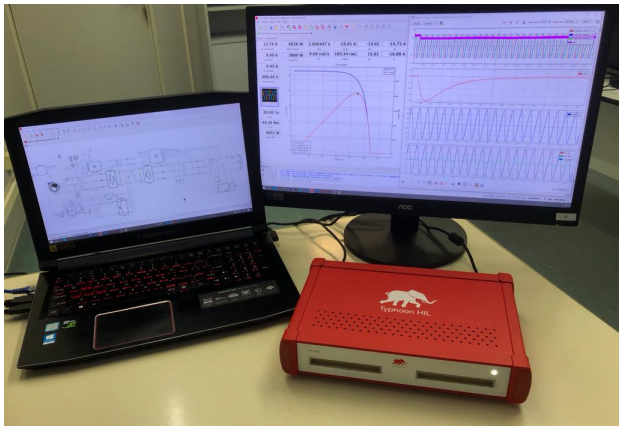

FIGURE 10. Typhoon HIL workspace for real-time simulation.

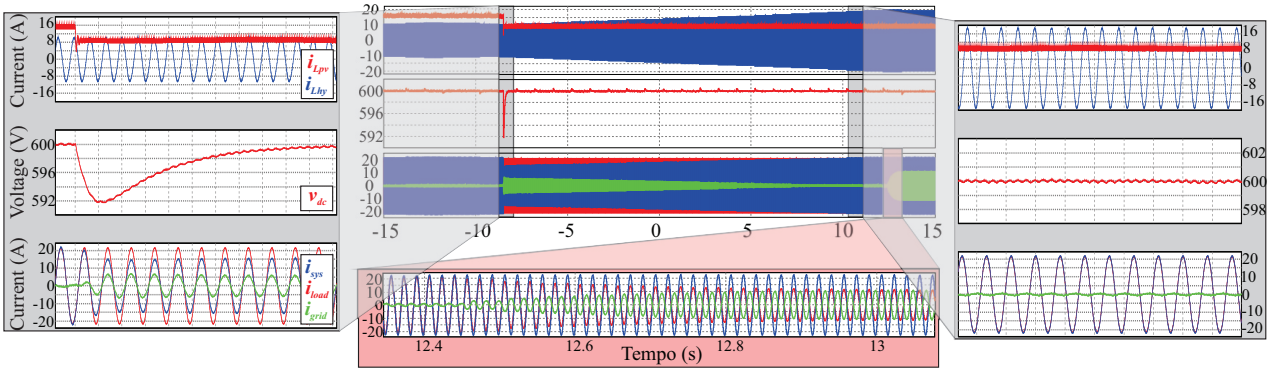

FIGURE 11. Source currents (i_{Lpv}, i_{Lhy}), bus voltage (v_{dc}) and PCC currents (i_{sys}, i_{load}, i_{grid}) during a decrease of irradiance/load.

A. Control analysis

Fig. 11 presents a 30-second simulation illustrating the slow dynamics of water energy and the system stabilization through grid energy input, along with the fast transient waveforms during decreases in irradiance and load, shown in a zoomed view.

The simulation demonstrates voltage control and reference tracking, highlighting the characteristics of the hydro genset along with the switched models of the converters under varying irradiance or load conditions. To maintain clarity, only the currents of the photovoltaic system and one phase of the hydro genset (i_{Lpv}, i_{Lhy}) are shown in the background, illustrated in the upper graphs. The central graph displays the dc bus voltage (v_{dc}) and its variation in response to the simulated irradiance step. The bottom graph shows the currents at the point of common coupling (PCC) of phase (a), including the current injected by the system (i_{sys}), the current consumed by the load (i_{load}), and the electrical grid current (i_{grid}). The graph clearly indicates that during the transition, the grid is responsible for maintaining stability.

The zoom in the transient performance of the dc bus control, on the left, shows the increase of the grid current to supply the instantaneous lack of energy. On the right, with the increase of the hydro genset current occurs the cancellation of the grid current. The time window in the highlighted red graph shows the current variations due to load variation. It can be seen that the generation is maintained, as the grid absorbs the excess generated to stabilize the system.

B. Comparative analysis

A long-term real-time simulation was conducted over 48 hours, using meteorological data to represent sunny and rainy days, with added irradiance reduction points simulating cloud cover or other obstructions to validate complementary control [21]. The simulation results, comparing the standard and proposed systems, are shown in Fig.12(a) and (b). The waveforms illustrate the system power injected into the grid (P_{SYS}), hydropower (P_{HYD}), and photovoltaic power (P_{PV}). Fig.12(b) also shows the reservoir level variation of the proposed system (Δh).

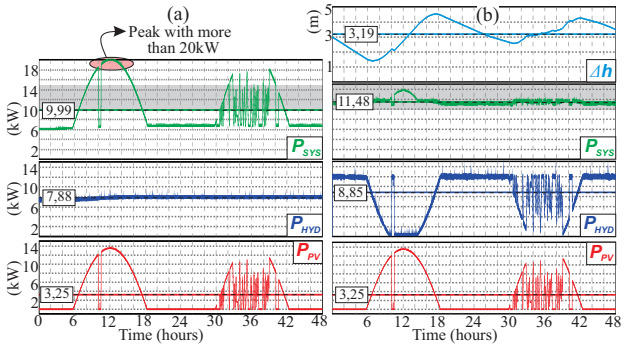

FIGURE 12. Power generation: (a) standard system; (b) proposed system.

During the first 24 hours illustrated in Fig.12, the average power generated by both systems is identical. The proposed system, however, shows less variation in instantaneous power. To evaluate this, a range of interest, shown in gray in Fig.12, was added to define the upper and lower limits of required generation. To avoid exceeding the distribution line generation limits in the standard system's, the power must be limited, as highlighted in Fig.12(a), whereas the proposed system remains within these limits. Additionally, the proposed system's reduced variation in instantaneous power indicates that it does not require energy exchange with the grid, offering economic benefits and a potential solution for off-grid operation, if a power control is applied.

On the second, rainy day, the proposed system gains an advantage due to increased water usage, maintaining the benefits seen in sunny conditions and confirming off-grid operation potential under varied weather. The average generation over 48 hours, shown as a constant line in each graph, highlights the hydro generation difference between the systems, with photovoltaic generation being identical.

C. Average model

Real-time simulation was also used to validate the average model obtained through the power of energy sources (3) and (15) represented in the block diagram of Fig. 13. While the PV generation follow (15), in the hydro generation the hydraulic loss coefficient (K_h) is added in block diagram,

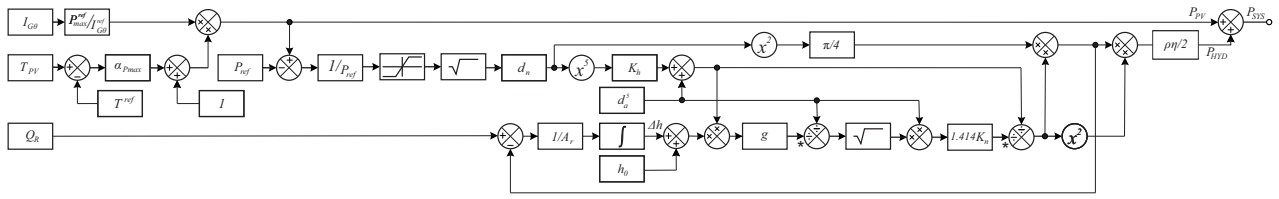

FIGURE 13. Proposed average model block diagram.

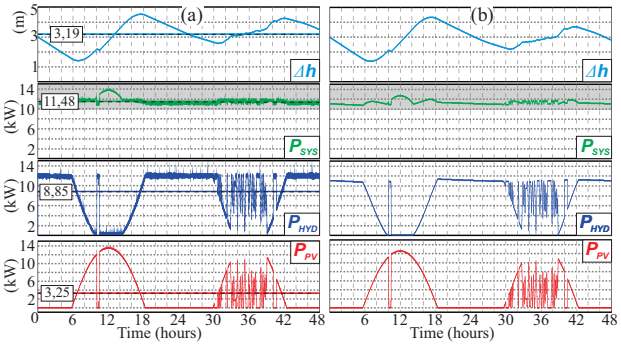

FIGURE 14. Proposed power generation: (a) real-time; (b) average model.

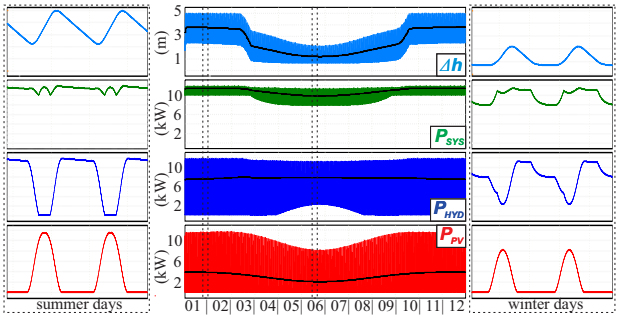

FIGURE 15. Yearly average model power generation simulation (26º35'S)

that is related with the parameters c_1, Q_e and Δh. Which is linked with length and friction factor of the pipeline, and loss nozzle coefficient by

$$K_h = f_a \cdot l_a \cdot K_n^2. \tag{30}$$

Using the same climatic data of the real-time simulation ($I_{G\theta}$, T_{pv}, Q_r), with the addition of the average model of the complementary control, were obtained the results shown in Fig. 14. These results demonstrate that the characteristics of power and variation of the level of the reservoir are preserved, thus validating the average model for an analysis in a longer period of simulation.

A long-term average model simulation was conducted over one year, with parameters predefined (T_0, H_0, Q_r, θ_α) following (8) and Fig. 13 average model block diagram. Solar energy nonlinearities (cloud, raining) weren't included, because of it is related with the luminosity index when (8) is applied. The generation waveforms results are shown in Fig. 15, with the daily average value of each graph in black. It highlights the system's behavior during summer, where is similar than real-time, and winter, where the reduction of reference of power was necessary to keep a minimum value of reservoir's level.

During the simulation the stream flow Q_r was kept constant, its increments by a raining period, could compensate the winter's lack of solar energy. Comparisons across different latitudes or changing the stream of river could be carried out, to evaluate the impact of this factor on the model, and find if the dispatchable characteristic could be achieved.

Generation capability clearly depends on the region's geographic and hydrologic conditions, as well as its climatic characteristics. The model developed in this paper aids in decision-making by evaluating if the conditions of a river in a particular region can enable dispatchable generation. It helps compare costs and assess sustainability, considering the system's goal of using hydro storage for dispatchable generation.

V. CONCLUSION

This paper has introduced a hybrid microgeneration approach that combines solar photovoltaic and hydro sources interconnected within a single dc bus, operating in parallel to create a more dependable energy source. This system demonstrates enhanced sustainability, particularly for off-grid applications, as it negates the necessity for battery usage.

The methodology employed for designing the converters and control mechanisms was succinctly outlined. Simulation outcomes reveal that under sunny conditions, both systems yield similar generation outputs. However, during rainy periods, the system showcases increased generation due to its ability to capitalize on heightened water flow resulting from rainfall, an advantage not achievable by standard systems limited by mechanical constraints. Consequently, it can be inferred that the proposed system exhibits greater generation efficiency in comparison to standard systems, particularly in regions experiencing higher rainfall.

A notable attribute of the derived average model, verified through hardware-in-the-loop simulation, is its ease of implementation. This model offers the convenience of evaluating the suitability of the proposed microgeneration system for a given region solely based on meteorological data available for that area.

ACKNOWLEDGEMENTS

The authors thank for the opportunity provided by the INCT-GD and Brazilians sponsors CNPq, CAPES, FAPERGS. 465640/2014-1,23038.000776/2017-54,17/2551-0000517-1.

AUTHOR'S CONTRIBUTIONS

DE PARIS, V.J.: Conceptualization, Data Curation, Formal Analysis, Investigation, Methodology, Project Administration, Resources, Software, Validation, Writing – Original Draft. **CARNIELUTTI, F.M.**: Conceptualization, Data Curation, Formal Analysis, Funding Acquisition, Investigation, Methodology, Resources, Software, Supervision, Validation, Visualization, Writing – Original Draft, Writing – Review & Editing. **MARTINS, D.C.**: Conceptualization, Formal Analysis, Funding Acquisition, Resources, Supervision, Visualization, Writing – Review & Editing.

PLAGIARISM POLICY

This article was submitted to the similarity system provided by Crossref and powered by iThenticate – Similarity Check.

REFERENCES

[1] REN21, "RENEWABLES 2021 GLOBAL STATUS REPORT", [Online], 2021, pp. 53, URL: https://www.ren21.net/wp-content/uploads/2019/05/GSR2021_Full_Report.pdf.

[2] M. S. Whittingham, "History, evolution, and future status of energy storage", *Proceedings of the IEEE*, vol. 100, no. SPL CONTENT, pp. 1518–1534, 5 2012, doi:10.1109/JPROC.2012.2190170.

[3] N. Lee, U. Grunwald, E. Rosenlieb, H. Mirletz, A. Aznar, R. Spencer, S. Cox, "Hybrid floating solar photovoltaics-hydropower systems: Benefits and global assessment of technical potential", *Renewable Energy*, vol. 162, pp. 1415–1427, 12 2020, doi:10.1016/j.renene.2020.08.080.

[4] E. Solomin, E. Sirotkin, E. Cuce, S. P. Selvanathan, S. Kumarasamy, "Hybrid floating solar plant designs: A review", *Energies*, vol. 14, no. 10, 2021, doi:10.3390/en14102751.

[5] Y. K. Choi, "A study on power generation analysis of floating PV system considering environmental impact", *International Journal of Software Engineering and its Applications*, vol. 8, no. 1, pp. 75–84, 2014, doi:10.14257/ijseia.2014.8.1.07.

[6] Y. Qiu, J. Lin, F. Liu, Y. Song, G. Chen, L. Ding, "Stochastic Online Generation Control of Cascaded Run-of-the-River Hydropower for Mitigating Solar Power Volatility", *IEEE Transactions on Power Systems*, vol. 35, no. 6, pp. 4709–4722, 2020, doi:10.1109/TPWRS.2020.2991229.

[7] D. Apostolopoulou, M. McCulloch, "Optimal Short-Term Operation of a Cascaded Hydro-Solar Hybrid System: A Case Study in Kenya", *IEEE Transactions on Sustainable Energy*, vol. 10, no. 4, pp. 1878–1889, 2019, doi:10.1109/TSTE.2018.2874810.

[8] Anuradha, S. K. Sinha, A. Yadav, "Modelling of DC linked PV/hydro hybrid system for rural electrification", *in 2017 Recent Developments in Control, Automation & Power Engineering (RDCAPE)*, pp. 55–59, 2017, doi:10.1109/RDCAPE.2017.8358239.

[9] K. O. Lawal, "Hydro-based, renewable hybrid energy sytem for rural/remote electrification in Nigeria", *in 2015 Clemson University Power Systems Conference (PSC)*, pp. 1–6, 2015, doi:10.1109/PSC.2015.7101691.

[10] Seema, B. Singh, "PV-Hydro-Battery Based Standalone Microgrid for Rural Electrification", *in 2018 5th IEEE Uttar Pradesh Section International Conference on Electrical, Electronics and Computer Engineering (UPCON)*, pp. 1–6, 2018, doi:10.1109/UPCON.2018.8597005.

[11] T. C. Singh, G. Satyaprasad, K. C. Rath, P. S. Rajesh, A. Kumar, "Solar PV based PSH system Performance evaluation and analysis for runoff river Pico hydro plant", *in 2020 IEEE International Symposium on Sustainable Energy, Signal Processing and Cyber Security (iSSSC)*, pp. 1–6, 2020, doi:10.1109/iSSSC50941.2020.9358851.

[12] S. Zhang, Y. Xiang, J. Liu, J. Liu, J. Yang, X. Zhao, S. Jawad, J. Wang, "A regulating capacity determination method for pumped storage hydropower to restrain PV generation fluctuations", *CSEE Journal of Power and Energy Systems*, vol. 8, no. 1, pp. 304–316, 2022, doi:10.17775/CSEEJPES.2020.01930.

[13] J. Yang, J. Liu, S. Zhang, "Optimization for Short-Term Operation of Hybrid Hydro-PV Power System Based on NSGA-II", *in 2020 IEEE 4th Conference on Energy Internet and Energy System Integration (EI2)*, pp. 2267–2271, 2020, doi:10.1109/EI250167.2020.9346601.

[14] J. Driesen, F. Katiraei, "Design for distributed energy resources", *IEEE Power and Energy Magazine*, vol. 6, no. 3, pp. 30–39, may 2008, doi:10.1109/MPE.2008.918703.

[15] M. F. Akorede, H. Hizam, E. Pouresmaeil, "Distributed energy resources and benefits to the environment", *Renewable and Sustainable Energy Reviews*, vol. 14, no. 2, pp. 724–734, 2010, doi:10.1016/j.rser.2009.10.025.

[16] Hidreo, "Hidreo", Online, 2021, URL: https://hidreo.com.br/.

[17] Turbulent, "Turbulent", Online, 2021, URL: https://www.turbulent.be/.

[18] V. F. Barbosa, A. O. C. Neto, G. B. Lima, D. B. Rodrigues, "Análise e Desenvolvimento de um Retificador Híbrido Monofásico Bidirecional com Compensação Série no Barramento CC para Aplicações em Microrredes", *Eletrônica de Potência*, vol. 25, no. 3, p. 305–315, Sep. 2020, doi:10.18618/REP.2020.3.0027.

[19] S. L. S. L. Dixon, C. A. C. A. Hall, *Fluid mechanics and thermodynamics of turbomachinery*, 7 ed., Elsevier, Oxford - UK, 2014, ISBN:978-0-12-415954-9.

[20] V. J. D. Paris, *Projeto e Simulação de um Sistema de Microgeração Híbrido Alimentado por Energia Hídrica e Solar Fotovoltaica*, Master's thesis, Federal University of Santa Catarina - UFSC, Florianópolis, Brazil, 2020.

[21] INMET, "Instituto Nacional de Meteorologia", Online, 2022, URL: https://portal.inmet.gov.br/.

[22] D. Goswami, F. Kreith, *Energy Efficiency and Renewable Energy Handbook*, 2 ed., Taylor & Francis, New York - USA, 2016, ISBN:978-1-4665-8509-6.

[23] A. Smets, K. Jäger, O. Isabella, R. van Swaaij, M. Zeman, *Solar energy The physics and engineering of photovoltaic conversion, technologies and systems*, 1 ed., UIT Cambridge Ltd., Cambridge - England, 2016, ISBN:978-1-906860-75-2.

[24] R. W. Erickson, D. Maksimovic, *Fundamentals of Power Electronics*, 2nd ed., Kluwer Academic Publishers, Massachusetts - USA, 2001, ISBN:978-0-306-48048-5.

[25] X. Ruan, X. Wang, D. Pan, D. Yang, W. Li, C. Bao, *Control Techniques for LCL -Type Grid- Connected Inverters*, Springer, 2018, doi:10.1007/978-981-10-4277-5.

[26] K. Ogata, *Discrete-Time Control Systems*, 2 ed., Prentice-Hall International, New Jersey - USA, 1995, ISBN: 0-13-328642-8.

[27] H. Akagi, E. H. Watanabe, M. Aredes, *Instantaneous Power Theory and Applications to Power Conditioning*, Wiley-IEEE Press, 2017, doi:10.1002/9781119307181.

[28] V. J. De Paris, F. De Morais Carnielutti, D. C. Martins, "A Sustainable Energy Storage System for Hydro-PV Microgeneration", *in 2023 IEEE 8th Southern Power Electronics Conference and 17th Brazilian Power Electronics Conference (SPEC/COBEP)*, pp. 1–8, 2023, doi:10.1109/SPEC56436.2023.10408091.

BIOGRAPHIES

Valdecir Junior De Paris , received B.S. degrees in mechanical/electrical engineering (2011/2018), an M.B.A. degree in lean manufacturing (2013) and an M.S. degree in power electronics (2022). He is currently a Ph.D. student with co-supervision at the federal university of Santa Catarina (Brazil) and Roma Tre University (Italy). His interest research areas include ac-dc/dc-ac converters, high frequency, power factor correction, distributed generation systems and microgrids. Valdecir Junior De Paris is a Member of the Brazilian Power Electronics Association (SOBRAEP).

Fernanda de Morais Carnielutti , (Member, IEEE) received the B.S., M.S. and Ph.D. degrees in electrical engineering in the Federal University of Santa Maria (UFSM), Santa Maria, Brazil, respectively in 2010, 2012 and 2015. From 2016 to 2018, she was a Professor with the Federal University of Santa Maria, campus Cachoeira do Sul. She is currently a Professor with the Federal University of Santa Maria, campus Santa Maria and a Researcher with the Power Electronics and Control Research Group (GEPOC), UFSM.

Her research interests include control and modulation of static power converters, multilevel converters, power electronics for renewable energies, microgrids and model predictive control. Dra. Carnielutti is a member of the IEEE Power Electronics Society, IEEE Industrial Electronics Society, and IEEE Industry Applications Society.

Denizar Cruz Martins , received the B.Sc. and M.Sc. degrees in electrical engineering from Federal University of Santa Catarina, Florianopolis, SC, Brazil, in 1978 and 1981, respectively, and the Ph.D. degree in electrical engineering from the Polytechnic National Institute of Toulouse, Toulouse, France, in 1986. He is currently a Full Professor and the Head of Power Electronics Institute in the Department of Electrical and Electronics Engineering at Federal University of Santa Catarina. His interest research areas include dc-dc and dc-ac converters, high frequency, soft commutation, power factor correction, grid-connected PV systems, distributed generation systems and dc/ac microgrids.